Vietnam Journal of Earth Sciences, 46(1), 48-68, https://doi.org/10.15625/2615-9783/19459

Vietnam Journal of Earth Sciences
https://vjs.ac.vn/index.php/jse

Geotechnical properties of natural sand-mixed granulated blast furnace slag applied to the sand compaction pile method

Nguyen Thi Thanh Nhan[1], Hiroshi Matsuda[2], Duong Trung Quoc[1], Tran Xuan Thach[1], Tran Thi Phuong An[1], Tran Thi Ngoc Quynh[1], Tran Thanh Nhan[1*], Pham Van Tien[3], Nguyen Thi Le Huyen[1]

[1]*University of Sciences, Hue University, 77 Nguyen Hue, Hue City 530000, Vietnam*
[2]*Yamaguchi University, 2-16-1 Tokiwadai, Ube, Yamaguchi 755-8611, Japan*
[3]*Institute of Geological Sciences, Vietnam Academy of Science and Technology, Hanoi 100000, Vietnam*

Received 20 July 2023; Received in revised form 22 September 2023; Accepted 21 November 2023

ABSTRACT

Granulated blast furnace slag (GBFS) has more advantageous properties over natural sand, such as lightweight, higher shear strength, and higher permeability. Therefore, it is regarded as a potentially promising substitute for natural sand in the ground improvement using the sand compaction pile (SCP) method. Due to the relatively rapid solidification, however, which is induced by the latent hydraulic property of GBFS, the permeability of the installed GBFS compaction pile (GBFSCP) decreases quickly, and such an application becomes difficult for the case of SCP with low sand replacement area ratio (LSRAR). So, to decelerate the permeability reduction of GBFSCP, different GBFSs, and natural sands were collected in Japan and Vietnam, and the specimens were prepared by changing the mixing ratio of sand to GBFS from 20% to 80%. Then, firstly, fundamental geotechnical properties of sand-mixed GBFS without hydration were observed. Secondly, the specimens of sand-GBFS mixture were cured in seawater at the temperature of 80°C for 3 days to 380 days. The unconfined compressive strength, permeability, and hydration reaction rate of the hydrated sand-mixed GBFS specimen were measured.

In conclusion, the geotechnical properties of the unhydrated sand-mixed GBFS become more advantageous than those of natural sand. In addition, by mixing with natural sand, the hydration reaction rate and the solidification of GBFS are controlled. This means that it is possible to keep the compressive strength and the permeability at the predetermined conditions and, in turn, to satisfy requirements for the SCP method with LSRAR. In addition, a simple estimation method of the unconfined compressive strength was proposed for the hydrated sand-mixed GBFS specimen.

Keywords: Geotechnical properties, granulated Blast Furnace Slag (GBFS), hydraulic property, permeability, sand compaction pile, unconfined compressive strength.

1. Introduction

In the production process of pig iron by melting iron ore and auxiliary materials (including limestone and coke) in the blast furnace, Blast furnace slag (BF slag) is produced with an average production of about 29%–30% by mass of the pig iron (in Vietnam, this rate is about 35%). BF slag is divided into two categories, Air-cooled blast furnace slag (ABFS) and Granulated blast furnace slag (GBFS), by cooling the molten slag naturally in open pits (or yards) and under high-pressure water, respectively. In

*Corresponding author, Email: ttnhan@hueuni.edu.vn

Japan, the annual production of BF slag and GBFS has exceeded 23 and 20 million tons since 2000, respectively (NSA, 2017). In Vietnam, the steel industry has developed quickly, resulting in a considerable increase in iron slag and steel slag production, exceeding 12 million tons since 2020 (a tenfold increase since 2013) (Nhan et al., 2022). In the Central region of Vietnam, the Formosa steel plant (Ha Tinh province) and Hoa Phat Dung Quat steel plant (Quang Ngai province), which are the two giant steel plants in Vietnam, currently produce over 4 million tons of BF slag annually in which, over 95 percent of BF slag is used to produce GBFS. On the other hand, construction in Vietnam currently faces a severe shortage of natural aggregate. In 2020, the annual usage of natural sand for construction in Vietnam was about 182-195 million m^3, adapted natural sand was only 50%-65% of the requirement, and natural river sand for construction would be exhausted in 10-15 years (Nga, 2017; Nguyen et al., 2018; Nhan et al., 2020).

Despite the large production amount of BF slag, since its chemical components are stable and satisfy the environmental requirements, this by-product has been used in many fields such as the cement industry, agriculture, construction civil works, etc. In comparison with natural sand, GBFS shows better physico-chemical properties such as high permeability (the permeability coefficient of $k \approx 10^{-3}$ m/s), lightweight (particle density of ρ_s = 2.30–2.70 g/cm^3), high internal friction angle ($\phi \geq 35^o$ for almost all the void ratio and $\phi > 40^o$ when the relative density of $D_r \geq 60\%$) (Matsuda, 2015). The dry density of GBFS under the standard compaction test is almost independent of water content, suggesting easier compaction management at the construction site (Matsuda, 2015; Nhan et al., 2019; 2022). When the natural sand is replaced by GBFS, the earth pressure of the backfill of quay walls, retaining walls, landfills, and embankments is reduced (Sato et al., 2008). Furthermore, GBFS possesses an inherent hydraulic property, resulting in it solidifying and experiencing a gradual increase in shear strength with time when exposed to natural wet conditions, all without the need for additives. It is anticipated to become a non-liquefiable material after a 6-month hardening period (Kikuchi, 1998; Shinozaki, 2006; Nakanishi et al., 2018; Matsuda et al., 2016; Wada et al., 2016). The physico-chemical characteristics of GBFS during its hydration process have been elucidated under various environmental conditions, including in-situ case studies (Matsuda et al., 1998; 2000; 2003; 2008; 2012; 2015; Wada et al., 2015; 2016). After being hardened, even when GBFS is collapsed, its shear strength is confirmed to be recovered. The recoverable shear strength and self-healing characteristics due to the so-called "secondary hydration reaction" have been confirmed even GBFS had been applied for an in-situ embankment over 11 years in the natural condition (Matsuda et al., 2015).

In the realm of soft ground improvement through the sand compaction pile (SCP) method with a low sand replacement area ratio (LSRAR) (LSRAR is defined as the cross-sectional area of the sand pile on the horizontal plane below A_s = 40%), the surcharge load is jointly supported by both the sand piles and the clay layer. Consequently, the permeability of the sand pile plays a crucial role in dissipating pore water pressure and consolidating the clay layer over time (Kitazume, 1994). Due to its advantageous physico-mechanical properties when compared to natural sand and its shear strength development over time due to hydration, GBFS is considered a promising alternative material for the SCP method. Conversely, it has been established that the hardening of GBFS is significantly influenced by grain refinement, particularly particle

crushing induced during the SCP construction. The greater the extent of GBFS particle crushing, the faster the increase in strength and the decrease in permeability (Shinozaki et al., 2006; Nakamura, 2016). Recent applications of GBFS in the SCP method have revealed that GBFS compaction pile (GBFSCP) can considerably reduce permeability to 10^{-6} cm/s. This reduction is attributed to the solidification of GBFSCP, which is partly accelerated by the compaction during the construction of GBFSCP. As a result, the dissipation of pore water from the clay layer through GBFSCP becomes constrained. This limitation makes the application of GBFSCP with LSRAR more challenging (Shinozaki, 2006; Mizuno, 2008). As an alternative approach, it is recommended to utilize GBFSCP as a drainage pile in the short term and as a high-strength pile in the long term (Sato et al., 1982).

To address this issue, particularly in mitigating the premature solidification of GBFSCP, GBFS samples sourced from different steel mills were collected and mixed with different natural sands at a mixing ratio ranging from r = 20% to r = 80%. The geotechnical properties of the unhydrated sand-GBFS mixtures were observed and compared with those of natural sands. Furthermore, sand-mixed GBFS specimens at a relative density of D_r = 80% were cured in seawater at a temperature of T = 80°C for a curing period ranging from t = 3 days to t = 380 days. The unconfined compressive strength, permeability, and hydration reaction rate of hydrated specimens were measured and combined with data from our previous research (Matsuda et al., 2015; 2016; Matsuda and Nhan, 2016) for a more comprehensive analysis. A method for estimating unconfined compressive strength was then proposed as a function of r and t. This method can be referenced to design an appropriate natural sand-GBFS mixture for the SCP method with LSRAR, tailored to the consolidation characteristics of any given soft soil layer.

2. Experimental Aspects

2.1. Testing materials

For this study, original samples of GBFS were sourced from two steel plants, one in Vietnam (symbolized as VGBFS) and the other in Japan (symbolized as JGBFS). The VGBFS samples were obtained from the Formosa steel plant, while the JGBFS samples were collected and preserved at the Geotechnical LAB of Yamaguchi University in Japan. Figure 1 displays photographs of the GBFS samples and a scanning electron microscope (SEM) image of a JGBFS particle.

Additionally, two types of natural sands, Genkai sand from Japan and Huong sand from Vietnam, were blended with GBFS. Genkai sand, a marine sand collected and previously employed in research (Matsuda et al., 2015; Nakamura, 2016), was selected. Huong sand, a river sand collected from the middle stream of the Huong River in Thua Thien Hue province, is currently in use as a fine aggregate for concrete within the province.

The tested materials' grain size and index properties are presented in Fig. 2 and Table 1, respectively. Original (unhydrated) GBFS particles show a coarse sand-like appearance. Still, on a microscopic scale, they appear more angular, with closed pores inside and open pores on the surface, as depicted in Fig. 1(c). Figure 2 illustrates that even VGBFS and Huong sand have slightly smaller grain sizes than those of Japanese ones, but such differences among the materials are negligible.

Regarding the observed results in Table 1, the index properties of both GBFS samples and the natural sands used in this study exhibit significant similarities. While GBFS exhibits a higher particle density than natural sand, its elevated porosity and surface roughness contribute to a significantly higher void ratio, leading to increased permeability and reduced dry density in GBFS specimens at the same relative density (D_r = 80%). These observations demonstrate the advantage of using GBFS as a substitute for natural sand in the SCP method.

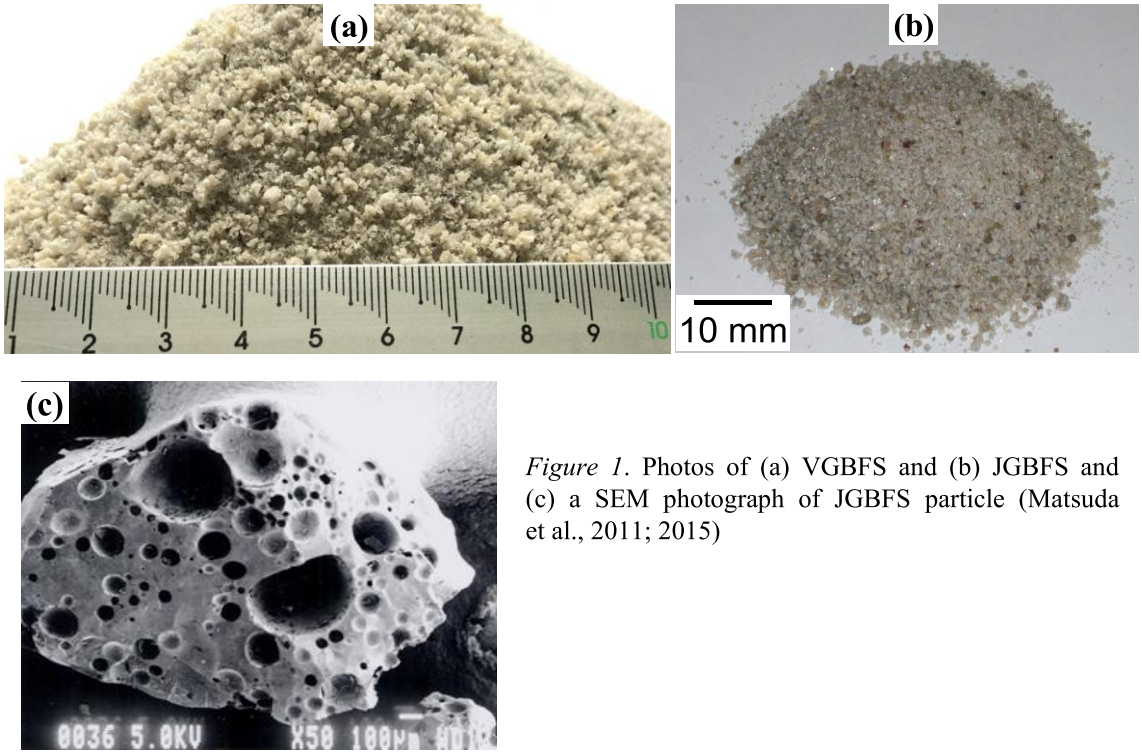

Figure 1. Photos of (a) VGBFS and (b) JGBFS and (c) a SEM photograph of JGBFS particle (Matsuda et al., 2011; 2015)

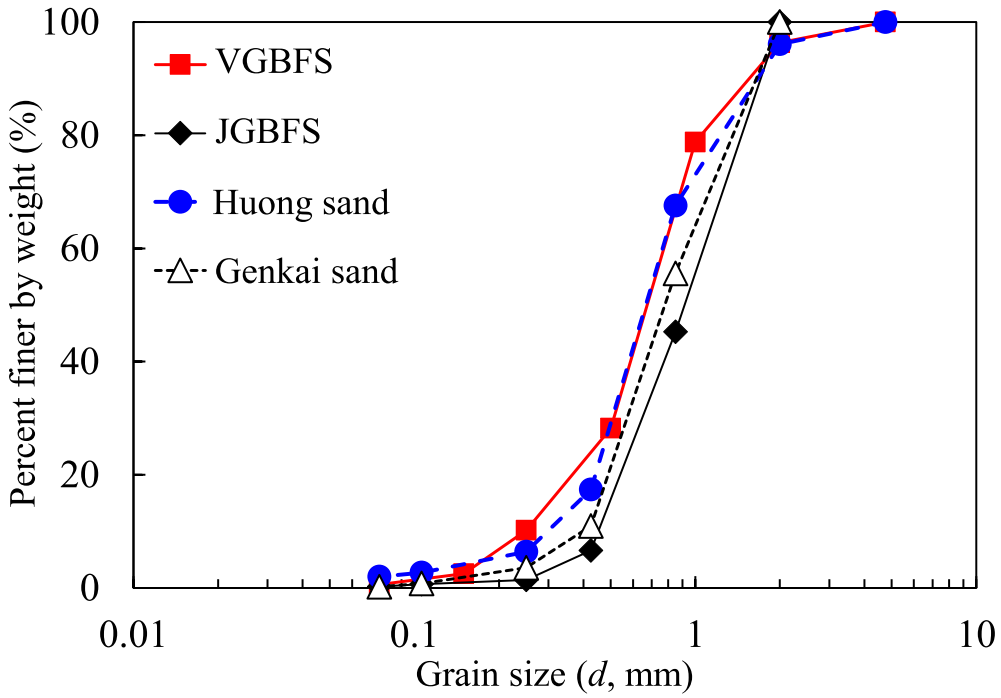

Figure 2. Grain size distribution curves of used materials

Table 1. Index properties of tested materials

Properties	VGBFS	JGBFS	Huong sand	Genkai sand
Particle density, ρ_s (g/cm^3)	2.790	2.705	2.661	2.650
Maximum void ratio, e_{max}	1.398	1.242	0.802	0.885
Minimum void ratio, e_{min}	0.881	0.866	0.493	0.615
Dry density at D_r = 80%, ρ_d (g/cm^3)	1.406	1.393	1.711	1.588
Void ratio at D_r = 80%, e	0.984	0.941	0.555	0.669
Permeability coefficient at D_r = 80%, k (×10^{-3} m/s)	1.35	2.86	0.21	1.11
Loss of Ignition, *IL* (%)	0.150	0.231	0.067	4.213

To prepare the sand-GBFS mixture, Genkai sand was blended with JGBFS, and Huong sand was combined with VGBFS in a range of mixing ratios from r = 20% to r = 80%. Here, r represents the ratio of the mass of natural sand to the total mass of the sand-GBFS mixture. The mass of GBFS at D_r = 80% served as the baseline value for calculating the mass of GBFS and natural sand for each mixing ratio. Subsequently, the geotechnical properties of Huong sand-VGBFS mixture and Genkai sand-JGBFS mixture were evaluated and compared with the original GBFS sample (i.e., r = 0%) and sand (i.e., r = 100%) in the following section.

2.2. Specimen Preparation and Curing Conditions

The solidification of GBFS and its latent hydraulic properties were investigated to determine its impact on shear strength and permeability. This investigation considered various curing conditions, such as tap water, seawater, and $Ca(OH)_2$ solution, at both room temperature (20°C) and 80°C. Natural conditions were also examined (Matsuda et al., 1998; 2000; 2003; 2008; 2012; 2015; Wada et al., 2015; 2016). To further understand these properties when JGBFS is mixed with natural sand for potential use in the SCP method with LSRAR, several testing series using the original JGBFS sample (r = 0%) and mixtures of Genkai sand-JGBFS at r = 20% to r = 80% were conducted. Test specimens were prepared as follows: predetermined masses of the samples for D_r = 80% were placed in plastic bottles and mixed with seawater at a solid-to-liquid ratio of 1:1.4. The mixture was left to sit with the lid on for one day before being de-aired in a vacuum cell. Subsequently, the de-aired mixture was poured into a plastic mold with dimensions of 50 mm in diameter and 100 mm in height using the water pluviation method. Images of typical GBFS and sand-mixed GBFS specimens can be seen in Fig. 3.

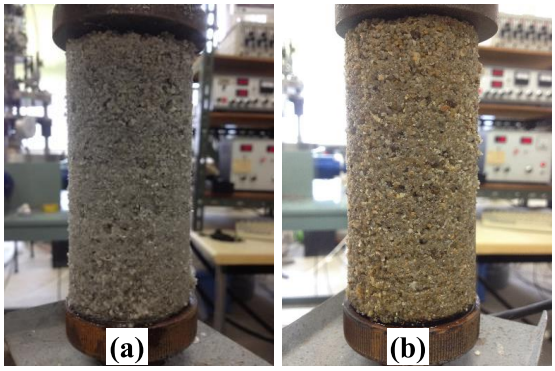

Figure 3. Typical specimens of (a) GBFS (r = 0%) and (b) sand-GBFS mixture at r = 80%

The hardening of GBFS is temperature-dependent as it relies on forming hydrates driven by chemical reactions. To expedite the hydration reaction rate of GBFS, specimens were immersed in seawater at a temperature of T = 80°C. The curing durations were fixed at t = 0, 3, 7, 14, 28, 56, 84, 112, 140, 168, 225, 280, 300, and 380 days (0 days denoting unhydrated specimens). After each of these curing durations, the cured specimens underwent a falling head permeability test, an unconfined compression test, and a hydration reaction test.

2.3. The permeability test and unconfined compression test

Figures 4 and 5 provide an overview of the falling head permeability test and unconfined compression test carried out in this study. The permeability test was conducted following JIS A 1218, a methodology consistent with our previous research (Matsuda et al., 2008; Matsuda and Nhan, 2016; Nhan et al., 2020; 2022). The testing procedures for both GBFS and sand-GBFS mixtures were similar. Specifically, the permeability test was executed at three different water head levels: 5 cm, 10 cm, and 20 cm, with three tests conducted at each level to obtain the testing results. The unconfined compression test was run at a constant strain rate of 1% per minute until failure was observed.

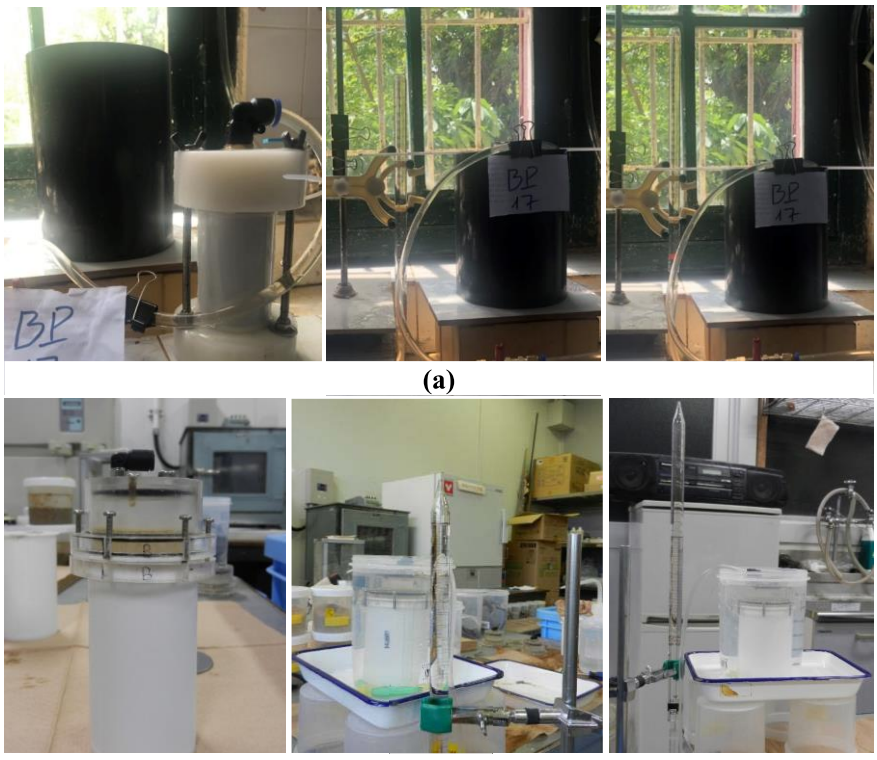

Figure 4. Typical falling head permeability tests carried out in (a) Vietnam and (b) Japan

Figure 5. Photos of typical unconfined compression tests on specimens of (a) GBFS specimen and sand-GBFS mixtures

2.4. Hydration reaction test and calculation method of the hydration reaction rate

In this study, the hydration reaction test was used to quantify the formation of hydrates during the solidification of JGBFS and a Genkai sand-JGBFS mixture. This method, initially proposed by Kondo and Ohsawa (1969), has been adopted in various research studies (Shinozaki et al., 2006; Matsuda et al., 2015; 2016; Nakanishi et al., 2018; Nhan et al., 2020; Wada et al., 2015; 2016). To ensure the accuracy of the test, we exclusively utilized specimens that had undergone unconfined compression tests, following the procedures illustrated in Fig. 6. Upon completing the compression test, the wet sample was carefully collected and dried at the temperature of 110°C for 1 day; hydration reaction test was then carried out as follows: 1 g of dried sample was precisely obtained and poured into a stoppered Erlenmeyer flask. The sample was mixed with a compound solution of 70 mL of acetone, 30 mL of methanol, and 5 g of salicylic acid before being agitated for an hour using a magnetic stirrer at 350 rpm (Fig. 6a). After keeping for 24 hours, the mixture was separated by vacuum filtration with quantitative filter paper at a 1.0 μm pore diameter. The obtained residues, together with the filter paper, were put into a crucible (Fig. 6b). To incinerate the filter paper for measuring the mass of the residues, the crucible was heated at 850°C for an hour (Fig. 6c).

Figure 6. Procedure of the hydration reaction test: (a) 1 g of dried sample was precisely obtained, mixed with a compound solution, and agitated by a magnetic stirrer in the stoppered Erlenmeyer flask; (b) a suction filtration separated the mixture, and the residues together with the filter paper were put into a crucible, (c) the residues were heated at 850°C for one hour before weight measurement

The hydration reaction ratio denoting the hydration reaction rate of JGBFS and Genkai sand-JGBFS mixture was then determined by Eqs. (1) and (2) as follows:

$$R_i = \frac{m_h}{m_d \times 1 - \left(\frac{IL}{100}\right)} \quad (1)$$

$$R = 100 - R_i \quad (2)$$

where R_i (%) is the un-hydrated ratio; m_d (g) is the mass of the dried sample before the test; m_h (g) is the mass of the residues after heating; IL (%) is the loss of ignition of the original JGBFS; and R (%) is the hydration reaction ratio.

In this study, specimens of JGBFS and Genkai sand-mixed JGBFS were cured in seawater, leading to the deposition of salinity on the surfaces of GBFS and sand particles. Consequently, the hydration reaction ratio, as calculated by Eqs. (1) and (2) might be overestimated due to dissolved salinity. Therefore, R_i should be calculated using Eq. (3), which excludes the mass of salinity (m_{sa}, g) from the tested sample.

$$R_i = \frac{m_h}{m_d \times 1 - \left(\frac{IL}{100}\right) - m_{sa}} \quad (3)$$

3. Results and Discussion

3.1. Geotechnical properties of sand-GBFS mixtures

3.1.1. The grain size and physical properties of natural sand-GBFS mixtures at different mixing ratios

Sandy soils are widely employed as conventional filling materials in the SCP method. To illustrate the enhancement of physical properties when mixing sand with GBFS, we observed the grain size and several index properties of sand-GBFS mixtures, comparing them with Huong sand and Genkai sand. As shown in Fig. 7, the grain size of all tested samples and mixtures is presented alongside the required grain size for filling material in sand drains, as per the Vietnamese standard (TCVN-11713:2017). It is seen that the grain size of natural sand slightly changes when mixed with GBFS, and all mixtures meet the requirements outlined in TCVN-11713:2017. Specifically, they contain more than 50% (by weight) with a diameter greater than 0.5 mm and less than 10% with a diameter less than 0.14 mm.

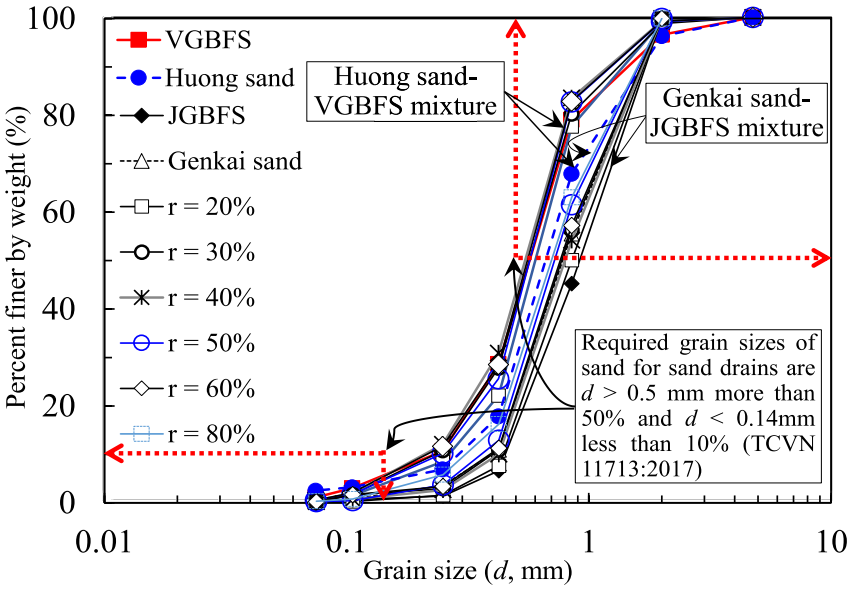

Figure 7. Grain size distribution curves of used materials and mixtures

Table 2. Physical properties of sand-GBFS mixtures

Mixture	Mixing ratio (r, %)	Particle density, ρ_s (g/cm^3)	Dry density at D_r = 80%, ρ_d (g/cm^3)	Maximum void ratio, e_{max}	Minimum void ratio, e_{min}	Void ratio at D_r = 80%, e	Permeability coefficient at D_r = 80%, k (×10^{-3} m/s)
Huong sand-VGBFS	20	2.726	1.569	1.021	0.667	0.738	0.612
	30	2.695	1.574	0.958	0.651	0.712	0.625
	40	2.685	1.592	0.901	0.633	0.687	0.823
	50	2.673	1.628	0.880	0.583	0.642	0.728
	60	2.665	1.644	0.827	0.569	0.621	0.501
Genkai sand-JGBFS	20	2.694	1.395	1.178	0.870	0.931	1.27
	30	2.689	1.440	1.155	0.796	0.868	1.35
	40	2.683	1.444	1.097	0.798	0.858	1.36
	50	2.642	1.501	1.044	0.689	0.760	1.30
	60	2.638	1.511	0.999	0.683	0.746	1.28
	80	2.643	1.553	0.948	0.640	0.701	1.40

The physical properties of all mixtures, including density (particle density (ρ_s, g/cm^3) and dry density at D_r = 80% (ρ_d, g/cm^3)), void ratio (at maximum and minimum conditions (e_{max} and e_{min}), and D_r = 80% (e)), and the permeability (at D_r = 80% (k ×10^{-3} m/s)) are summarized in Table 2. Changes in these properties concerning r are depicted in Figs. 8 and 9 in which, the results of the original GBFSs (i.e., r = 0%) and sands (i.e., r = 100%) are also included. Although some scattering in the observed permeability results exists, it is evident that that ρ_d increases for all mixtures while ρ_s, k, and the void ratio (e_{max}, e_{min} and e) generally decrease as r increases. Therefore, compared to natural sand, a conventional material for the SCP method, the sand-GBFS mixture, as an alternative, becomes lighter with a higher void ratio and greater permeability. These trends become more pronounced as r increases. In essence, adding GBFS enhances the properties of sand, aligning it with the intended qualities required for filling material in the SCP method.

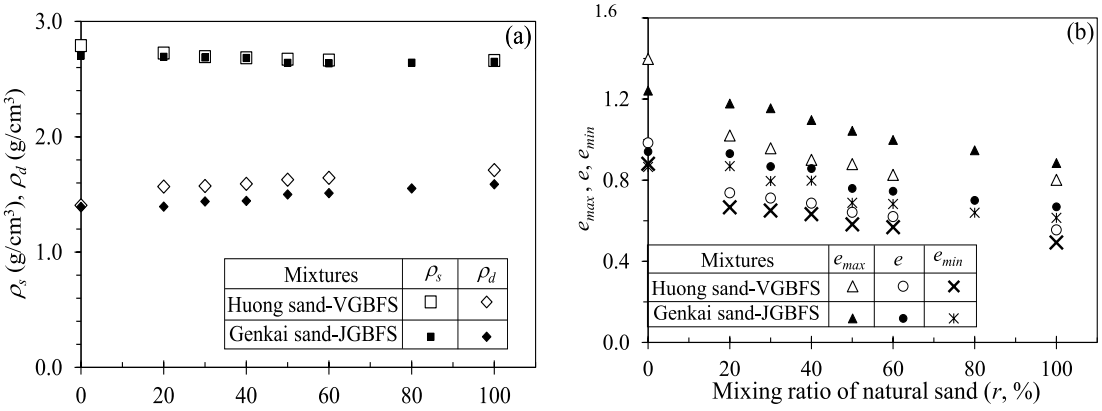

Figure 8. Changes in physical properties of sand-GBFS mixture with the mixing ratio (r, %)

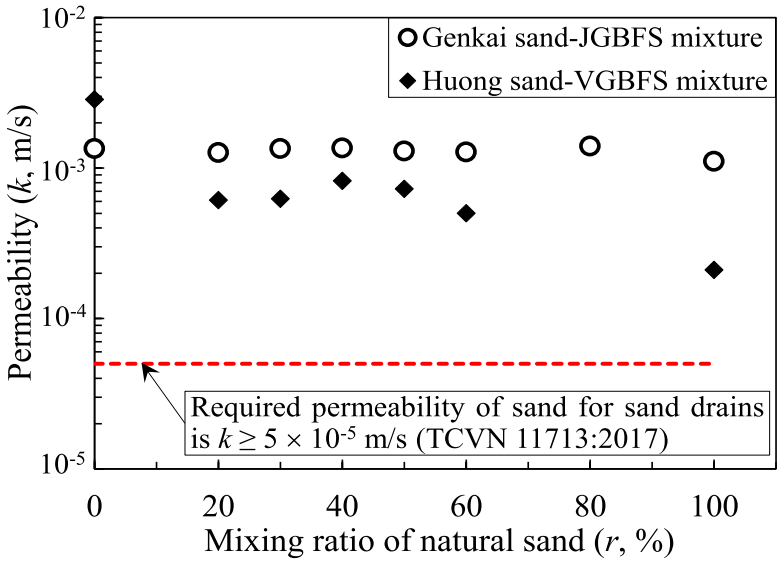

Figure 9. Changes in the permeability (k, m/s) of sand-GBFS mixture with r

3.1.2. Compaction curves of the sand-GBFS mixture

The variations in ρ_d concerning the water content (w, %) in the standard compaction test for GBFS (comprising VGBFS and JGBFS), natural sands (Huong sand and Genkai sand), and all mixtures of Huong sand-VGBFS are illustrated in Fig. 10.

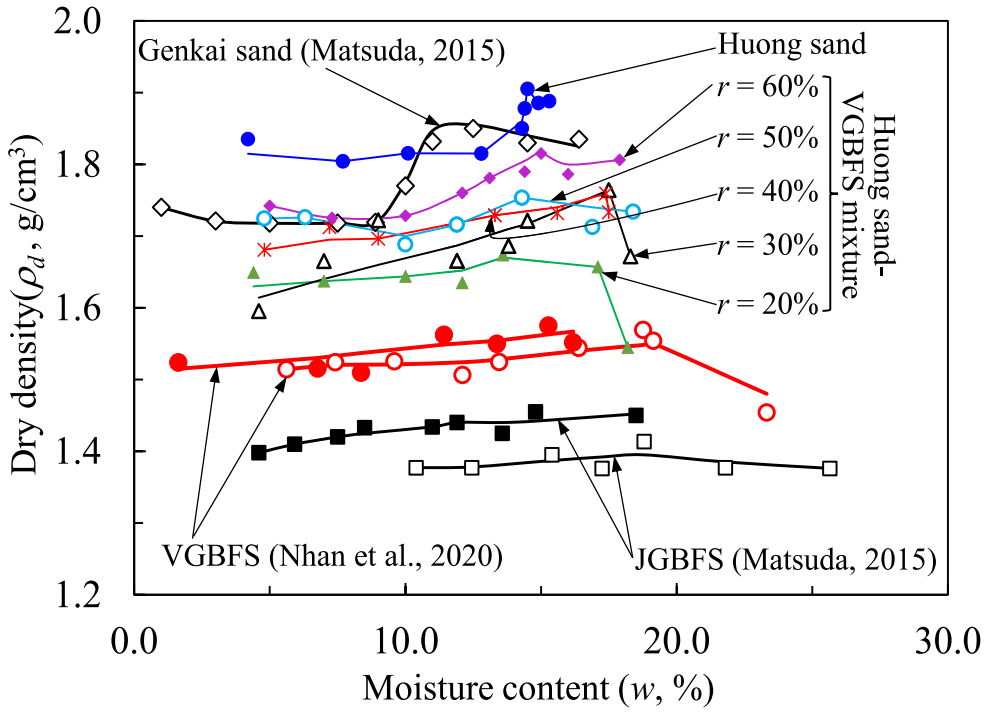

Figure 10. The standard compaction test curves of tested materials and mixtures

The results for Genkai sand and JGBFS were previously reported by Matsuda (2015), while data for VGBFS was obtained from the study conducted by Nhan et al. (2020). The standard compaction test involved three compaction layers, a 2.5 kg rammer, and 25 compaction times per layer. Typical compaction curves with a peak indicating maximum dry density and the optimal water content are evident in the case of Genkai sand and Huong sand. In contrast, for VGBFS and JGBFS, ρ_d exhibits a slight upward trend with increasing water content, but the differences in ρ_d remain negligible, even across a wide range of water content (e.g., from w = 5% to 20%). This behavior is also observed in the sand-GBFS mixture. Under identical water content and compaction conditions, JGBFS and VGBFS exhibit lower ρ_d values than natural sands.

Consequently, the ρ_d of the Huong sand-VGBFS mixture increases with the mixing ratio (r). The observations in Fig. 10 suggest that ρ_d of GBFS and the sand-GBFS mixture is less influenced by the water content during the compaction process. This implies that compaction management becomes easier, and the compaction pile becomes lighter when GBFS is utilized as an alternative material, either in part or entirely, in the SCP method compared to natural sand.

3.2. Changes in the physicomechanical properties of hydrated sand-GBFS mixture

3.2.1. The hydration reaction of Genkai sand-JGBFS mixture

The previously acquired geotechnical properties indicate that the unhydrated GBFS-sand mixture has the potential to serve as a promising alternative material for the SCP method. As changes in the physico-mechanical properties of GBFS have been elucidated through its hydration process under various curing conditions, the mixture of JGBFS and Genkai sand at the same mixing ratio was subjected to curing in seawater at T = 80°C for a duration ranging from t = 0 days (means unhydrated mixture) to t = 380 days. The unconfined compressive strength, the permeability, and the hydration reaction rate of the hydrated mixture were subsequently observed.

Figure 11 shows the changes in R with t for JGBFS (r = 0%) and all mixtures of Genkai sand-JGBFS. The results reveal a consistent upward trend in R as t increases, regardless of r. When comparing the results for each mixing ratio up to $t \leq 100$ days, it becomes evident that the higher the proportion of natural sand, the lower the hydration reaction rate. In the case of r = 80%, R remains nearly zero even as the curing duration surpasses t = 100 days. However, when $t \geq 100$ days, the mixtures at r = 30%-50% show the highest R values. This phenomenon could be attributed to the significant presence of shell fragments in Genkai sand, which might expedite the hydration reaction of JGBFS after a certain period of immersion in seawater at elevated temperatures. It is important to note that this phenomenon warrants further investigation from a chemical reaction perspective, which falls outside the scope of the current research.

Given that the original JGBFS sample contains an initial hydrated component, the hydration reaction ratio increment (ΔR, %) was used to account for and eliminate this component, as specified by Eq. (4).

$$\Delta R = R - R_0 \quad (4)$$

where R_0 is the original hydration reaction ratio of the JGBFS sample.

Consistently employing the same symbol for each mixing ratio of marine sand, as depicted in Fig. 11, the alterations in ΔR are graphed against t in Fig. 12. Just as observed in Fig. 11, it is evident that ΔR increases proportionally with t. Furthermore, when t exceeds 100 days, the mixtures at r = 30%-50% exhibit the highest ΔR values.

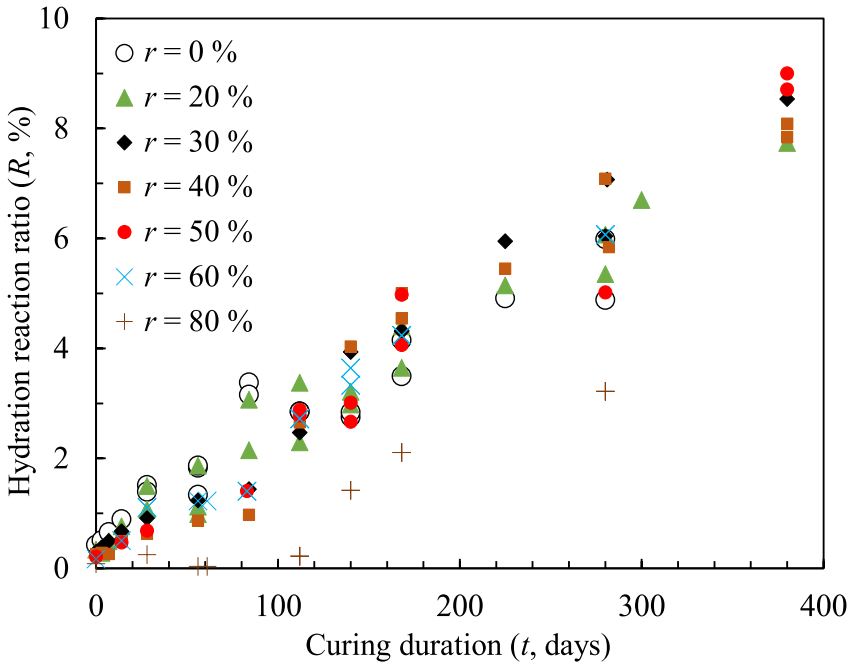

Figure 11. Increasing tendencies of the hydration reaction ratio (R, %) with curing duration (t, day) when Genkai sand-JGBFS mixture cured in seawater at T = 80°C

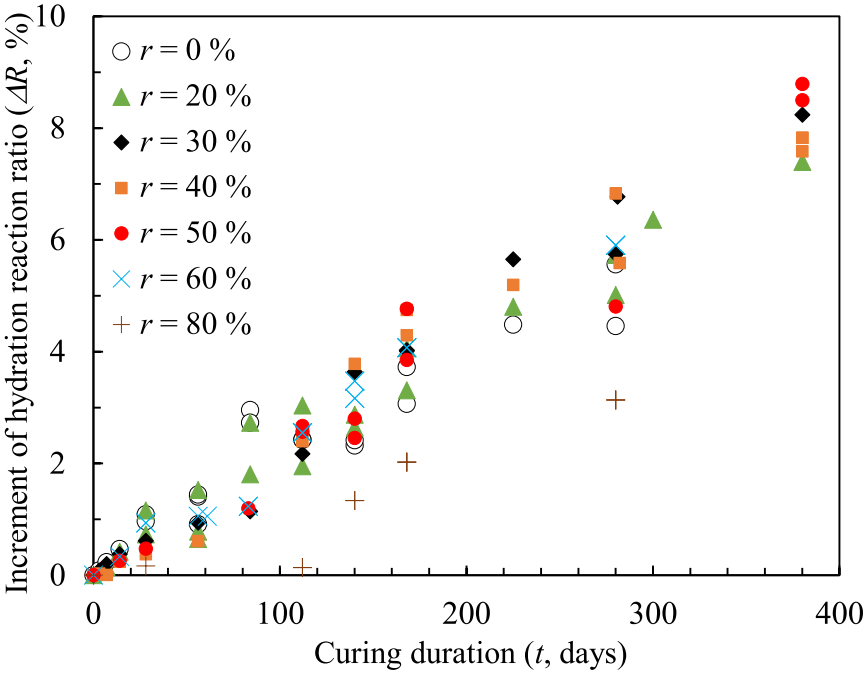

Figure 12. Relationships between the increment of hydration reaction ratio (ΔR, %) and t when Genkai sand-JGBFS mixture cured in seawater at T = 80°C

To delve into the impact of combining Genkai sand with JGBFS in greater detail, the normalized hydration reaction ratio (R_n, %) was used. Subsequently, the changes in R_n are plotted against t in Fig. 13 for all tested specimens. The definition of R_n, according to Eq. (5), is as follows:

$$R_n = \frac{R}{\left(1 - \frac{r}{100}\right)} \quad (5)$$

With the utilization of R_n, it becomes evident that the greater the proportion of Genkai sand in the mixture, the more substantial the increase in the normalized hydration reaction ratio of the Genkai sand-JGBFS mixture. Consequently, the addition of Genkai sand accelerates the hydration reaction of JGBFS, and this acceleration persists throughout the entire curing duration up to t = 380 days.

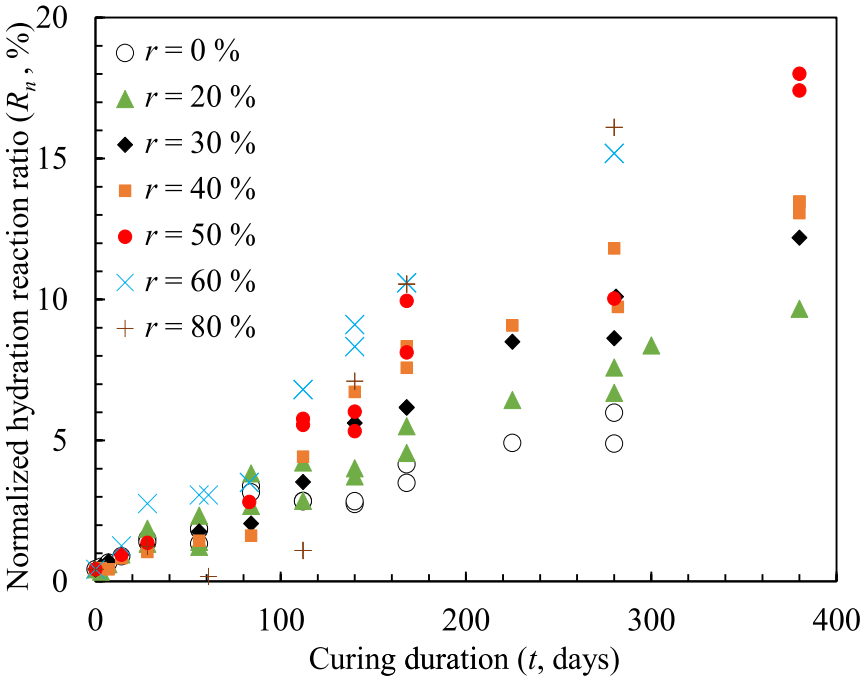

Figure 13. Relationships between the normalized hydration reaction ratio (R_n, %) and t for Genkai sand-JGBFS mixture cured in seawater at T = 80°C

3.2.2. The unconfined compressive strength of hydrated Genkai sand-JGBFS mixture

Figure 14 shows the variations in unconfined compressive strength (q_u, kN/m^2) with t for different mixing ratios of the Genkai sand-JGBFS mixture. It is noted that the specimens failed at r = 20% and t = 380 days during the testing procedure, rendering it impossible to obtain experimental results for q_u (as well as the permeability coefficient). The results suggest a general tendency of increasing q_u with t, and when $t \leq$ 140 days, q_u remains relatively low, with the influence of the mixing ratio being insignificant. However, when t exceeds 140 days, q_u noticeably rises with increasing r and reaches its peak values at r = 40%-50%, subsequently declining at the higher mixing ratios (i.e., $r \geq$ 60%).

As previously mentioned, the solidification and strength development of GBFS are significantly influenced by the hydrates formed during its hydration process. As a result, correlations between q_u and ΔR have been proposed in prior studies (Matsuda et al.,

2015; Matsuda and Nhan, 2016; Nakamura, 2016; Nhan et al., 2020). Based on these correlations, the relationships between q_u and ΔR is shown by symbols in Fig. 15 for all specimens used in this study. By employing ΔR instead of t, the increasing tendency of q_u, as indicated by the gray stripe, becomes more prominent, regardless of the values of t and r. Furthermore, in addition to the findings in Fig. 15, it is observed that the strength of the hydrated sand-mixed GBFS specimen initiates an increase when ΔR reaches or exceeds 2%. This suggests that ΔR = 2% can be considered as the threshold hydration reaction ratio for the strength build-up of the sand-GBFS mixture used in this study.

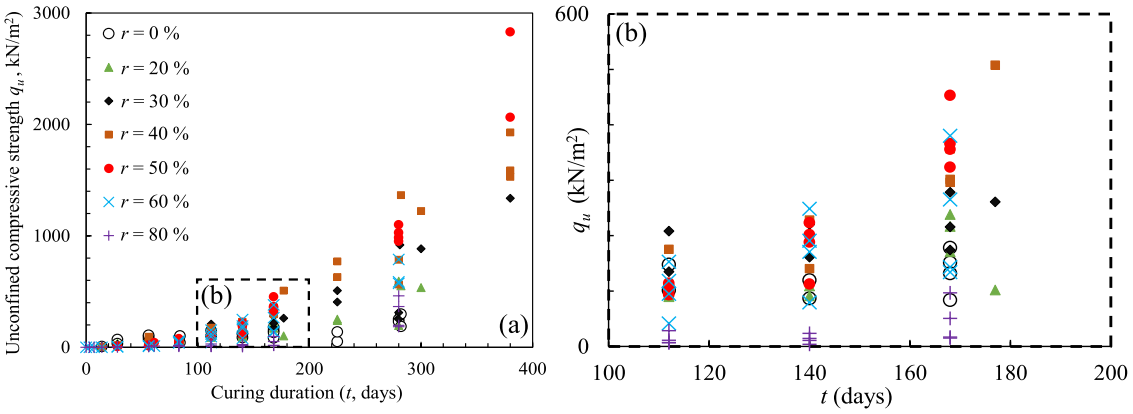

Figure 14. a-Relationships between the unconfined compressive strength (q_u, kN/m^2) and t for Genkai sand-JGBFS mixtures cured in seawater at T = 80°C, b-enlarge from the dashed rectangular (b) in figure (a)

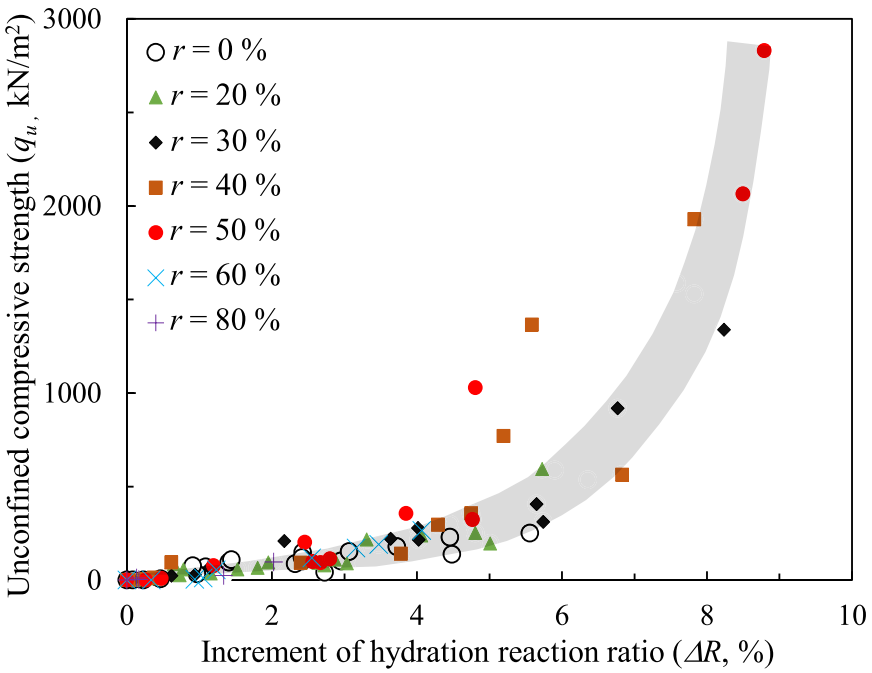

Figure 15. Relationship between q_u and ΔR for Genkai sand-JGBFS mixtures cured in seawater at T = 80°C with t = 0 to 380 days

3.2.3. The permeability of hydrated Genkai sand-JGBFS mixture

In Fig. 16, changes in the permeability coefficient (k, m/s) with t are shown across a range from r = 0% (representing the original JGBFS) to r = 80%. The symbols in Fig. 16 align with those used in previous figures depicting the experimental results, while the solid lines correspond to the fitting lines for each mixing ratio. Despite some scattering in the data points, it is evident that the permeability of the Genkai sand-JGBFS mixture changes within the range of $k = 10^{-3}$ m/s to 10^{-4} m/s, while the permeability of the original JGBFS can drop to approximately $k = 3\times10^{-5}$ m/s. Consequently, by introducing marine sand with a similar grain size (as shown in Fig. 1), the permeability of JGBFS increases with r, except for the case of r = 30%, where experimental results exhibit significant scattering. This tendency is consistent regardless of the curing period. Notably, mixtures with r = 40% to 50% show the most substantial increase in q_u over curing time, as demonstrated in Fig. 14. However, in Fig. 16, the permeability of such mixtures remains approximately at $k = 10^{-4}$ m/s. This observation has significant implications for the advantageous utilization of sand-GBFS mixture as an alternative filling material for the SCP method with LSRAR.

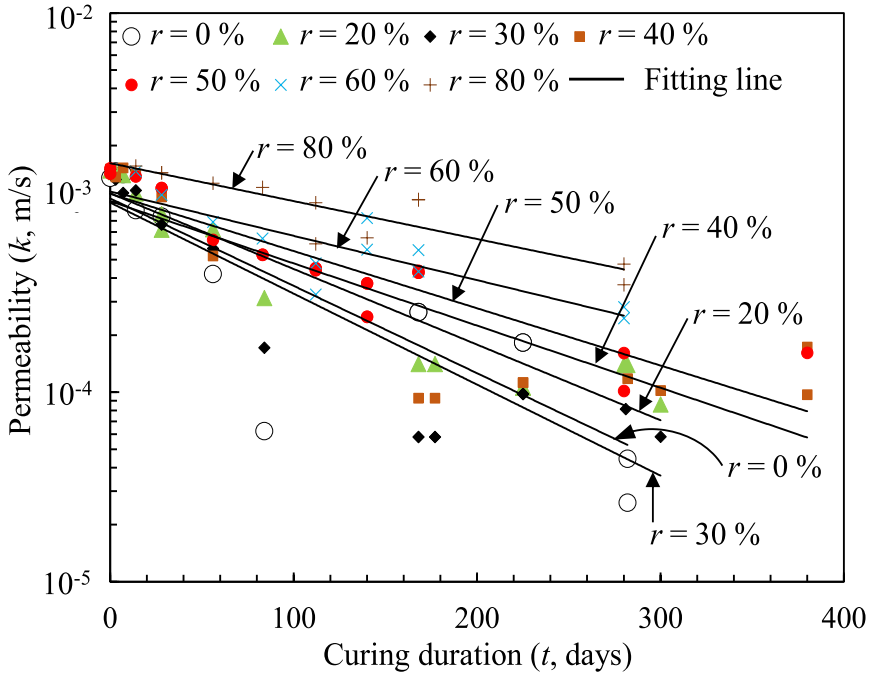

Figure 16. Changes in the permeability (k, m/s) with t when Genkai sand-JGBFS mixture cured in seawater at T = 80°C

To provide a more detailed examination of the influence of the JGBFS hydration rate on the permeability of the Genkai sand-JGBFS mixture, the changes in k with ΔR are shown by symbols in Fig. 17. The results reveal a general decline in k as ΔR increases, and the magnitude of this diminishing trend, indicated by the slope of the solid-fitting lines, notably diminishes as the mixing ratio increases from r = 0% to r = 60%. Beyond an r of 60%, the impact of the mixing ratio on the k-ΔR relationship

becomes negligible. Therefore, by incorporating marine sand, a dual advantage can be achieved: enhancing the unconfined compressive strength of JGBFS (which may reach 2000 kN/m^2) while maintaining its permeability at a satisfactory level (higher than k = 5×10^{-5} m/s, as per TCVN-11713:2017). This makes it a promising candidate for potential applications in the SCP method with LSRAR.

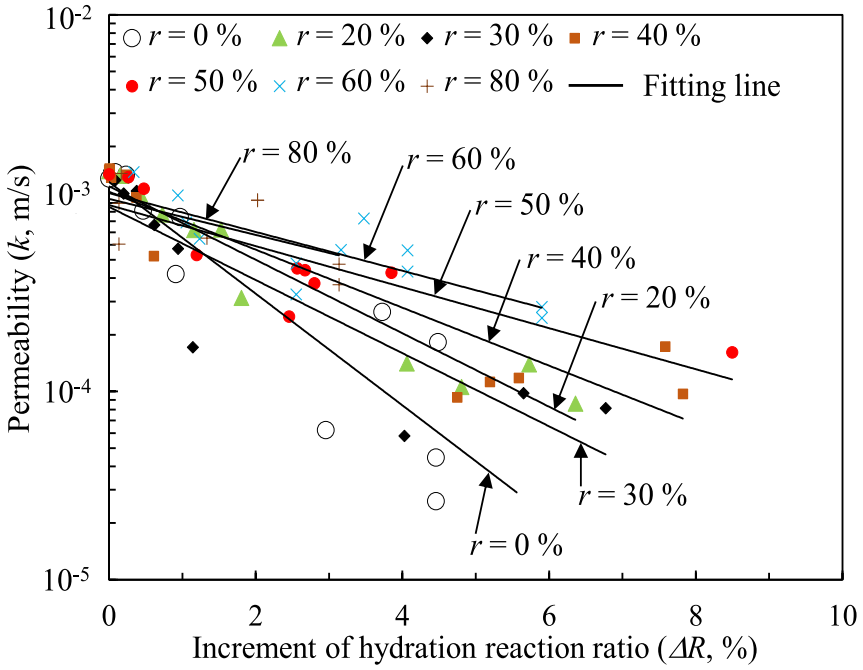

Figure 17. Relationships between k and ΔR for Genkai sand-JGBFS mixture cured in seawater at T = 80°C and for t = 0 day to t = 380 days

3.3. Estimation of the unconfined compressive strength of a hydrated sand-GBFS mixture

The inclusion of Genkai sand, which contains a high proportion of shell fragments (indicated by the high IL in Table 1), accelerates the hydration reaction of JGBFS, resulting in significant increases in ΔR and q_u, as observed in Figs. 12 and 14. However, when the mixing ratio becomes too high (e.g., $r \geq 60\%$), the surface area of JGBFS becomes smaller than that of Genkai sand. Consequently, the bonding between particles and the overall strength cannot fully develop within the mixture. This accounts for the decrease in ΔR and q_u of the mixture when r exceeds 60%. In other words, the potential application and the development of a method for estimating q_u in Genkai sand-JGBFS mixtures should be restricted to cases where r is less than or equal to 50%.

The variations in q_u with t, as depicted in Fig. 14, have been represented by symbols in Fig. 18 for r ranging from 0% to 50%. The solid lines in this figure represent fitting curves based on relationships outlined in Table 3, which express the correlations between q_u and ΔR as follows.

$$q_u = A \times t^B \quad (6)$$

where A and B are experimental constants.

To incorporate the influence of the sand mixing ratio into Eq. (6), the values of constants A and B obtained against r are represented by symbols in Fig. 19 while the solid lines in this figure illustrate the correlations between the experimental constants and r, as summarized in Table 4.

Table 3. Relations between q_u and t for different mixing ratios

Mixing ratio of Genkai sand, r (%)	Relations
0	$q_u = 0.0026 \times t^{2.2839}$
20	$q_u = 0.0278 \times t^{1.8312}$
30	$q_u = 0.1202 \times t^{1.4889}$
40	$q_u = 0.5488 \times t^{1.1337}$
50	$q_u = 2.5595 \times t^{0.7733}$

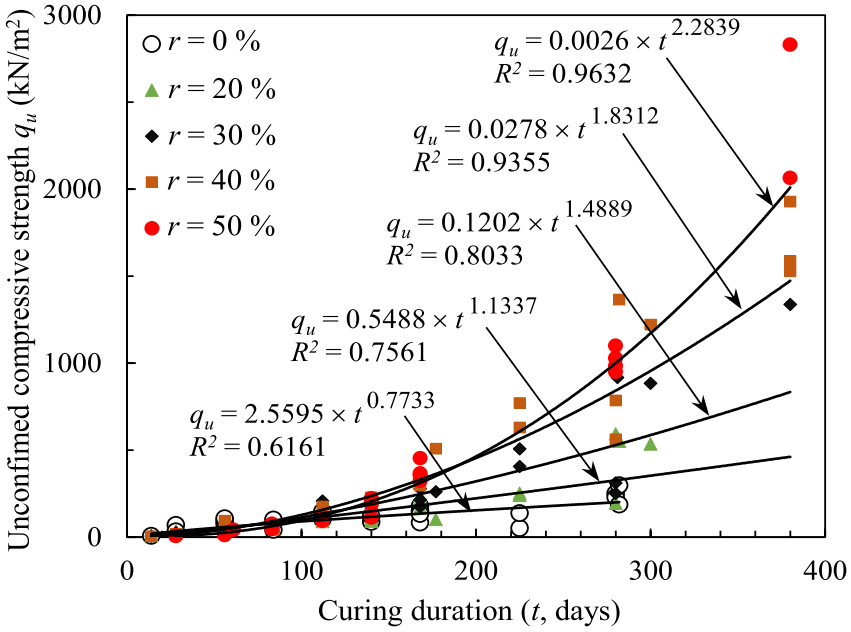

Figure 18. Relationships between q_u and t for Genkai sand-JGBFS mixture at r = 0% to 50%

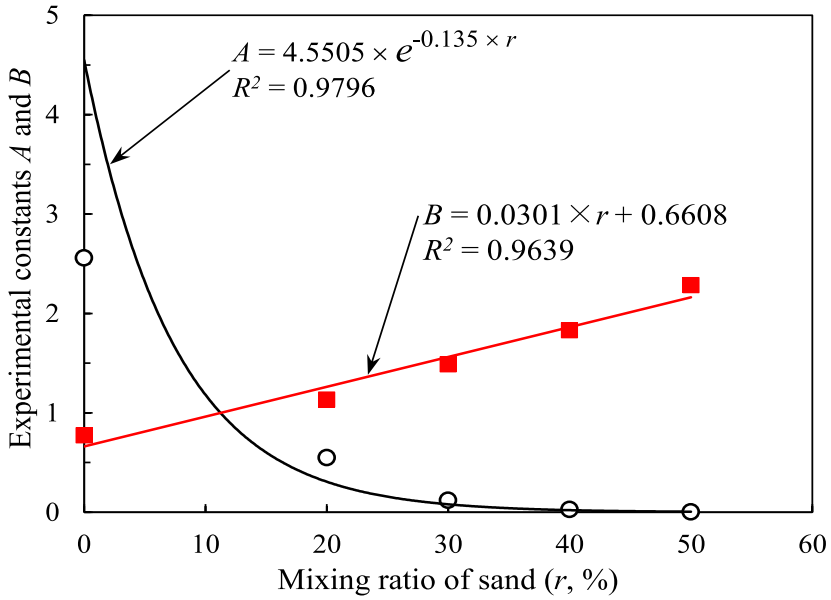

Figure 19. Changes of experimental constants A and B with r

Table 4. Relations between experimental constants A and B with r

Experimental constant	Relation
A	$A = \exp(-0.135 \times r) \times 4.5505$
B	$B = 0.0301 \times r + 0.6608$

By incorporating the obtained correlations from Table 4 into Eq. (6), the unconfined compressive strength of Genkai sand-mixed JGBFS can be expressed in terms of r and t. The results obtained for r = 0% to r = 50%, as shown in Fig. 14a, are represented again in Fig. 20a. In this figure, the symbols are the experimental results. At the same time, the solid curves correspond to the values calculated using Eq. (6). Comparisons between the observed and calculated results of q_u are further illustrated in Fig. 20b. Despite of some scattering in the data, reasonable agreements can be observed. As a result, the estimation of unconfined compressive strength using Eq. (6) is confirmed for Genkai sand-JGBFS mixture with a wide ranges of curing durations and mixing ratios.

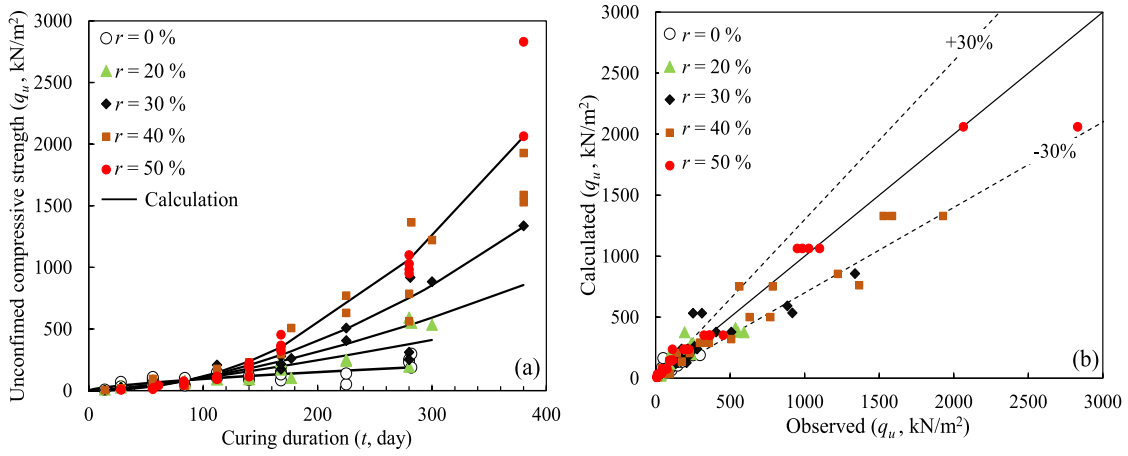

Figure 20. Comparisons between the observed and calculated results of q_u with curing duration t and for various sand mixing ratios

4. Conclusions

In this study, two unhydrated GBFSs were mixed with two natural sands at mixing ratios ranging from r = 20% to r = 80%. The objective was to investigate the geotechnical properties of the sand-GBFS mixture to determine its suitability as a substitute material in the SCP method. In addition, specimens with a D_r of 80% for a sand-GBFS mixture were cured in seawater at a temperature of T = 80°C. Over a curing period from t = 3 days to 380 days, the permeability, the compressive strength, and the hydration reaction rate were measured. A simple calculation method for the compressive strength was proposed based on r and t. The primary conclusions of this study are summarized as follows:

When natural sand is mixed with GBFS, ρ_d of the sand-GBFS mixture decreases as r decreases. Simultaneously, the void ratio (e_{max}, e_{min} and e) and k increase. Under equivalent compaction conditions, the ρ_d of the mixture is lower than that of natural sand and displays a greater degree of independence from w.

In seawater with T = 80°C, the hydration reaction rate in a sand-GBFS mixture, denoted as ΔR, exhibits a linear increase with t. When t surpasses 100 days, the mixture with r values between 30% and 50% shows the most substantial increase in ΔR.

The unconfined compressive strength of the sand-GBFS mixture displays a time hysteresis during its hydration process when compared to its hydration rate (ΔR). Initially, ΔR experiences a rapid increase immediately after curing, with the exception of the case where r = 80%. In contrast, q_u begins to build-up at $t \geq 112$ days and becomes notably more pronounced at $t > 140$ days. Subsequently, specimens with r values between 40 and 50% exhibit the most substantial increase in q_u and may reach q_u = 2000 kN/m^2 at t = 380 days. Moreover, when using ΔR instead of t, the tendency of q_u becomes even more distinctive, and ΔR = 2% can be considered as the threshold hydration reaction ratio for the strength development of the sand-GBFS mixture used in this study.

The permeability of the sand-GBFS mixture decreases with t, and at the same t, specimens with higher mixing ratios show higher permeability. When comparing the same value of r, k decreases with ΔR, and as r increases from r = 0% to r = 50%, the extent of this reduction in permeability diminishes. For $r \geq 60\%$, the influence of the sand mixing ratio on the decreasing relationships between k and ΔR becomes negligible.

The most significant increase in q_u with t was observed in the Genkai sand-JGBFS mixture at the mixing ratios between r = 40% and 50%; meanwhile, the permeability of this mixture retained at approximately $k \geq 10^{-4}$ m/s irrespective of the curing duration. Then, a simple method to estimate q_u as a function of both t and r was proposed for r = 0% to r = 50%. This estimation method can serve as a valuable reference when selecting an appropriate sand-GBFS mixture for the SCP method with LSRAR.

The findings in this study are exclusively derived from two natural sands, two GBFSs, and one specific curing condition (seawater at T = 80°C), which are known to expedite the hydration reaction of GBFS. Therefore, additional research is warranted to explore the behavior of various natural sands, GBFSs, and alternative curing conditions to obtain more comprehensive and generalized results.

Acknowledgments

This research was supported by Hue University through the Core Research Program, with Grant No. NCM.DHH.2018.03 and Grant No. DHH2021-01-185. Additionally, the experimental works received partial support from students who graduated from Yamaguchi University. The authors wish to extend their appreciation to these individuals.

References

Kitazume M., 1994. The sand compaction pile method with the low sand replacement area ratio. Tsuchi to Kiso, JGS, 42(1), 45–46.

Kikuchi Y., Takahashi K., 1998. Change of mechanical characteristics of granulated blast furnace slag according to age. Technical note of the port and harbor research institute, Ministry of transport, Japan, 915p.

Kondo R., Ohsawa S., 1969. Studies on a method to determine the amount of granulated blast furnace slag and the rate of hydration of slag in cements. Ceramics Association Journal, 77, 39–46.

Matsuda H., Kitayama N., Ando Y., Nakano Y., 1998. Effective utilization of granulated blast furnace slag in geotechnical engineering. Ground Engineering, 16, 33–40.

Matsuda H., Koreishi T., Kitayama N., Ando Y., Nakano Y., 2000. Engineering properties of granulated blast furnace slag. Coastal Geotechnical Engineering in Practice (IS-Yokohama 2000), 663–668.

Matsuda H., Ohira N., Takamiya K., Shinozaki H., Kitayama N., Murakami M., 2003. Application of granulated blast furnace slag to light weight embankment. Proc. of the international conference organized by British Geotechnical Association, 603–611.

Matsuda H., Shinozaki H., Ishikura R., Kitayama N., 2008. Application of granulated blast furnace slag to

the earthquake resistant earth structure as a geomaterial. Proc. of the 14th World Conference on Earthquake Engineering, Beijing, China, 12–17.

Matsuda H., Andre P.H., Ishikura R., Kawahara S., 2011. Effective stress change and post-earthquake settlement properties of granular materials subjected to multi-directional cyclic simple shear. Soils and Foundations, 51(5), 873–884.

Matsuda H., Ishikura R., Wada M., Kitayama N., Baek W., Tani N., 2012. Aging effect on the physical and mechanical properties of granulated blast furnace slag as lightweight banking. Japanese Geotechnical Journal, 7, 339–349.

Matsuda H., Hara H., Igawa N., Nakamura S., 2015. Evaluation of self-restoration characteristics of GBFS by using hydration reaction. The 15th Asian regional Conference on Soil Mechanics and Geotechnical Engineering, Fukuoka, Japan, JPN, 113.

Matsuda H., 2015. Application of granulated blast furnace slag as a geotechnical material. 2nd International Conference on Engineering Geology in Respond to Climate Change and Sustainable Development of Infrastructure, Hanoi, 75–84.

Matsuda H., Nakamura S., Nhan T.T., Hara H., Wada M., Ishikura R., 2016. Application of granulated blast furnace slag to the sand compaction pile method with low sand replacement area ratio. Proc. 69th Annual Canadian Geotechnical Conference - GeoVancouver 2016, Vancouver, Canada, 6p.

Matsuda H., Nhan T.T., 2016. Shear strength and permeability of granulated blast furnace slag mixed with marine sand from low to high mixing ratio. 2nd International Conference on Geological and Geotechnical Engineering in Response to Climate Change and Sustainable Development of Infrastructure, Hanoi, 63–70.

Ministry of Science and Technology of Vietnam (MOST), 2017. TCVN-11713:2017: Soft ground improvement by sand drains - Construction and acceptance, 27p.

Mizuno K., Tsuchida T., 2008. The finite element analysis on strength and deformation characteristics of improved ground by sand compaction pile method using the granulated blast furnace slag. Journal of Geotechnical Engineering, 3(3), 187–202.

Nakamura S., 2016. Effects of mixing sand with GBFS on the characteristics of hardening and permeability. Master thesis, Yamaguchi University, 44p.

Nakanishi J., Hara H., Matsuda H., Nhan T.T., Shinozaki H., 2018. The application of strength estimation technique on GBFS from different plants. Annual Conference of Japanese Geotechnical Society (JGS), 2018.

Nga T., 2017. Utilization of crushed sand: an inevitable trend. Electronic Newspaper of the Ministry of Construction on December 12, 2017. (https://baoxaydung.com.vn/su-dung-cat-nhan-tao-xu-huong-tat-yeu-221980.html).

Nguyen T.V., Nguyen M.T., Le A.T., 2018. A study on steel slag replacing sand in concrete. 4th International Conference on Green Technology and Sustainable Development (GTSD), November 23-24, Ho Chi Minh, 821–824.

Nhan T.T., Matsuda H., Thach T.X., Vien N.D., Thanh H.T., 2020. Strength of granulated blast furnace slag during hydration reaction process. Lecture Notes in Civil Engineering, 54, 427–432. Doi: https://doi.org/10.1007/978-981-15-0802-8_66.

Nhan T.T., Thach T.X., Vien N.D., Quoc D.T., Huy D.P., 2020. Physico-mechanical properties and chemical components of granulated blast furnace slag for the applicability as a recycled construction material. Proceedings of the 3rd Conference on Sustainable Earth, Mine, Environment (EME2020), Hanoi, 231–240.

Nhan T.T., Hai N.L.P., Thien D.Q., Nhan N.T.T., Thuy N.T., Thanh H.T., Cuong N.H., Huy D.P., Dat L.D., 2022. Study on the changes in the physico-mechanical properties with time and curing conditions for effective utilizations of granulated blast furnace slag in Ha Tinh. Report of Ha Tinh province level research project, 108p.

Nippon Slag Association (NSA), 2017. Statistical yearbook of iron and steel slag.

Sato Y., Matsuda H., Muraoka K., Kanazawa M., 2008. Soil Pressure Characteristics of Granulated Blast Furnace Slag Used as Backfill Material. Summary of the 43rd Geotechnical Research Conference, 549–550.

Sato Y., Koromo T., Fukuda Y., 1982. Geotechnical Properties of Granulated Blast Furnace Slag as Soil

Improvement Material and Their Changes Over Time. 37th Annual Conference of the Japan Society of Civil Engineers Lecture Abstracts III, 601–602.

Shinozaki H., Matsuda H., Sasaki E., Ono K., Suzuki M., Nakagawa M., 2006. Hardening property of granulated blast furnace slag and its application to soil improvement. Journal of JSCE, Division C, 62(4), 858–869.

Wada M., Matsuda H., Hara H., Igawa N., Nakamura S., 2015. Fundamental study on self-restoration characteristics of granulated blast furnace slag focusing on a hydration reaction. Journal of the Society of Materials Science, 64(7), 573–578.

Wada M., Matsuda H., Hara H., Nakamura S., Igawa N., 2016. Quantitative evaluation of strength and self-restorative capacity of granulated blast furnace slag. Journal of the Society of Materials Science, 65(1), 28–33.